COUNTERCURRENT FLOW LIMITATION IN VERTICAL DUCTS AT HIGH SYSTEM PRESSURES

M. Stephan and F. Mayinger

Lehrstuhl A für Thermodynamik
Technische Universität München, FRG

ABSTRACT

An experimental and analytical study on adiabatic countercurrent flow limitation (flooding) in single vertical ducts is reported. Experimental results on flooding curves, pressure drop and void fraction obtained with Freon 12 liquid and vapour in a rectangular channel are presented. The data were obtained under steady-state conditions, at various critical pressure ratios (0.16-0.31) and liquid injection flow rates, and alternatively using two different liquid feed locations. No substantial effect of the liquid injection location and flow rate on the liquid delivery (flooding) curves and on the pressure drop during flooding was found. The pressure drop data obtained at different elevations were essentially the same. Void fraction profiles evaluated from optical fiber probe data indicate an annular-type flow pattern. Based on this experimental evidence a mechanistic flow model is developed. The results are compared to the present high pressure and a number of comparable low pressure data sets, showing reasonable predictions of not only the flooding curves, but also the pressure drop during flooding.

1. INTRODUCTION

In vertical two-phase flow, the process of flooding leads to the limitation of the liquid downflow rate penetrating against a given gas or vapour upflow rate. Due to the variety of related applications in the chemical and nuclear industry, flooding has been the subject of numerous experimental and some analytical studies. The experimental work mainly focussed on adiabatic flooding in single channels, but also on the effects of multiple-path geometries or of interfacial condensation in case of subcooled liquid injection. Analytical models may be classified into three categories according to whether they are based on entrainment, wave instability or film flow mechanisms. Detailed reviews of these studies have been published by *Bankoff and Lee /1/* and by *Tien and Liu /2/*.

The most widely used tools to predict flooding are essentially empirically derived equations, such as the well-known *Wallis or Kutateladze* correlations */3/4/*. Generally these correlations give satisfactory results only for experimental conditions very similar to those, for which they have been developed, since the combined effects of crucial parameters, such as channel dimension, liquid viscosity and surface tension are not taken into account in detail. Moreover, various definitions of flooding have been applied in experimental studies. This may explain the observed spread among existing data and a number of incosistently reported effects on flooding, such as influences of the channel length and of the experimental procedure, which are related to particular definitions of the phenomenon.

The purpose of the present work is to contribute to the understanding of the flooding phenomenon in single channels under well-defined conditions. Therefore, the steady-state partial liquid delivery process is investigated. In this case, undesired secondary effects are less likely to affect the results than in a number of studies, where the applied flooding criteria were based on the onset of flow instabilities or liquid entrainment. At present, there is only few knowledge about the influence of pressure variations and of high system pressure on flooding, and the validity of known calculation methods in such cases is uncertain. More knowledge about steady-state flooding phenomena at high system pressures is particularly useful in the context of emergency core cooling analyses for pressurized water reactors. The use of Freon 12 as a modeling fluid allows to perform tests at high critical pressure ratios, with only moderate pressures and temperatures. Moreover, the Freon data support the evaluation of possible effects of fluid properties, such as surface tension and liquid viscosity, on flooding, and are thus helpful for the assessment of the analytical model presented in this paper.

2. EXPERIMENTAL APPARATUS

A schematic diagram of the closed test loop is given in figure 1. The rectangular test section is about 2 m long and mounted in a circular pressure vessel of 3 m height, shown by bold solid lines in the figure. The inlet and exit vapour flow rates are measured by vortex shedding flow meters, whereas turbine flow meters are used to measure the inlet liquid flow rate as well as the net liquid downflow and excess upflow rates.

Figure 2 shows a schematic diagram of the test section. The liquid is injected as a falling film via porous sinter plates mounted flush with one of the larger channel walls, at two alternatively used axial feed locations. Lateral view windows are installed for flow visualization. Differential pressure measurements were taken at four elevations, in the counterflow and the cocurrent flow region, using capacitance type differential pressure transducers. The distance between two successive pressure taps is 0.3 m.

At two axial locations, optical fiber probes are installed to measure the liquid fraction during flooding. The probes are horizontally adjustable by means of micrometer gauges. Figure 2 includes a scheme of the optical probe set-up. According to the different refractive indices of the phases contacting the probe tip (vapour or liquid), either

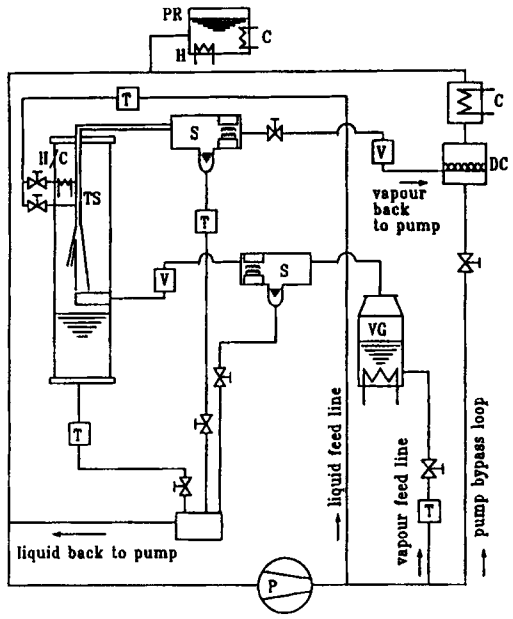

Fig.1 Test Loop

a very large or a very small fraction of the light intensity emitted versus the tip is reflected and then transformed into an analog output signal, which was sampled at a frequency of 20 kHz. The liquid fraction was evaluated from the time traces of this signal. The particular probe arrangement used in this study provides a very high vapour-to-liquid signal amplitude (≈10 V). The miniaturized probe tip (D ≈10 μm) allows the detection of very small droplets.

3. TEST CONDITIONS AND PROCEDURE

An overview of the experimental conditions covered in this paper is given in table 1. All test series included runs with various total liquid injection rates. In test series I and II, the liquid injection location was varied. The temperatures of the injected liquid and vapour were equal to the saturation temperature (adiabatic conditions). The test runs were generally performed by setting a fixed vapour flow rate and then adjusting the liquid injection flow rate to its desired value. This particular test procedure did not produce any ambiguity of the results, since it was found that neither various pathes of approach to flooding, such as setting the liquid flow first and then adjusting the vapour rate or vice versa, nor a very slow or stepwise approach to flooding conditions, did affect the measured operating points under steady-state conditions.

4. TEST RESULTS AND DISCUSSION

4.1. Flooding Curves

Figure 3 shows experimental flooding curves for three system pressures as solid, dot-dashed and dashed lines, respectively. The additional horizontal lines refer to

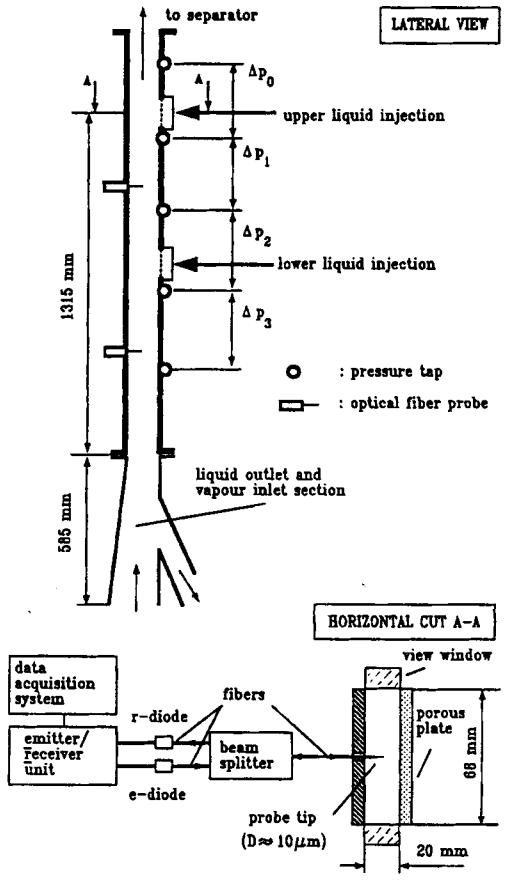

Fig.2 Test Section and Optical Probe Set-Up

p/p_{crit}=0.16 and connect the "stable" operating points, where all the liquid flow is downwards, for constant liquid injection rates j_L^{IN}. Due to the high upflow momentum caused by the high vapour densities, the vapour velocities necessary to cause flooding are very low compared to low pressure tests and decrease with increasing pressure.

Similar to previously reported results by *Kröning /5/, Celata et al. /6/, Zabaras and Dukler /7/8/* and other investigators, the present data reveal essentially no effect of the total liquid injection rate, i.e. of the excess upflow rate, on flooding. In the investigated flow rate range, this result was found irrespective of the system pressure and is shown for p/p_{crit}=0.16 in figure 3. However, *Kröning /5/* found that the flooding curves were shifted to lower gas velocities with increasing liquid injection rate, when using a weir instead of a porous plate feed. *Celata et al. /6/* reported the same trend for the highest liquid injection rate applied in their tests. Both these trends suggest that excessive liquid entrainment and carry-over near the liquid feed location may cause reduced downflow rates in case of high injection rates and/or unsuitable injection devices. Experimental flooding curves obtained under the influence of secondary effects of this type are clearly not comparable to data such as the present ones, where no effect of the liquid injection rate was found. The latter result indicates that the liquid downflow rate is inambiguously controlled by a flow limiting process within the channel.

Table 1 Test Conditions

TEST SERIES	NO.	I	II	III
system pressure, MPa	p	0.67	1.0	1.3
critical pressure ratio	p/p_{crit}	0.16	0.24	0.31
saturation temperature, C	$T_{C,sat}$	26	41.5	52.5
liquid density, kg/m^3	ρ_L	1305	1245	1198
vapour density, kg/m^3	ρ_V	38.0	57.1	74.9
phase density ratio	ρ_L/ρ_V	34.3	21.8	16.0
surface tension, N/m	σ	0.0086	0.0067	0.0052
liquid viscosity, 10^3kg/ms	η_L	0.21	0.18	0.15
channel cross section, $10^3 m^2$	A	———	1.36	———
channel hydr. diameter, 10^3m	D_E	———	30.9	———

As shown in figure 3, changes of the counterflow region length by alternatively using different liquid injection locations did not affect the measured flooding curves, in the present tests. In previous studies, effects of this length on flooding have generally been found, when flow pattern transitions at the approach to flooding were chosen as flooding criterion. (*Hewitt et al. /9/, McQuillan et al. /10/, Suzuki and Ueda /11/*). Observations by these investigators */10/11/* indicate that effects of the channel length are related to the increase of the liquid film waviness with the distance from the feed, causing a disturbed or chaotic flow pattern occuring at lower gas velocities for longer channels. However, the present results as well as data by *Zabaras and Dukler /7/* provide some evidence that there is no effect of the length on the steady-state liquid delivery process, which is investigated in this study.

4.2 Pressure Drop

Figure 4 provides some information on the pressure gradients in the counterflow region measured in test series I (p=0.67 MPa). The trends obtained at other system pressures are qualitatively the same. The error band with respect to the presented data is of the order of ±40 Pa/m.

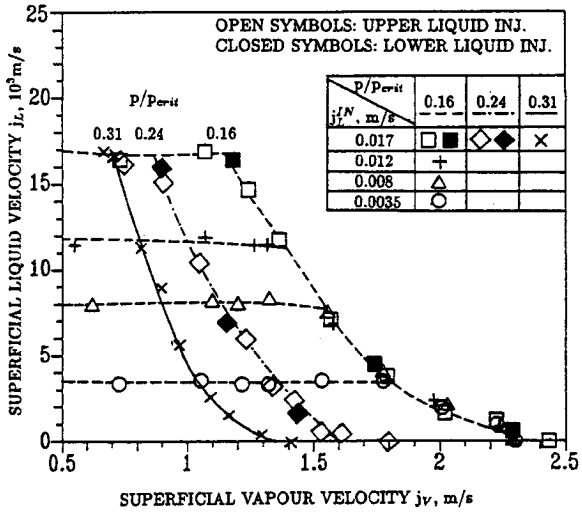

Fig.3 Flooding Curves

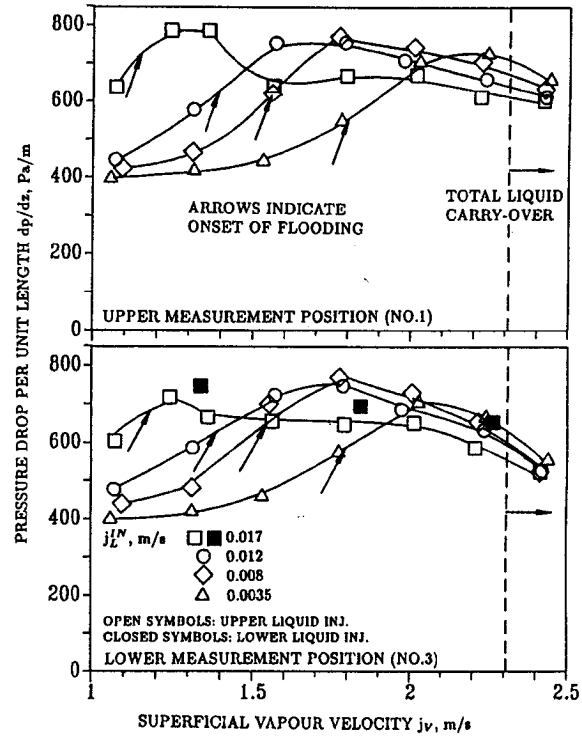

Fig.4 Pressure Drop at Different Measurement Positions (p=0.67 MPa)

The pressure drop characteristics are roughly independent of the liquid injection location and of the measurement position along the channel. This result suggests that the considered steady-state liquid delivery process is not governed by local phenomena at particular locations along the channel. For each liquid injection rate, the pressure drop increases in a range of gas velocities close to the onset of flooding and then reveals a slightly decreasing tendency up to the total liquid carry-over point, thus reflecting a decreasing interfacial momentum exchange or entrained liquid fraction, due to the gradually reduced liquid downflow rate.

The mentioned pressure drop increase around the onset of flooding is relatively flat and covers a wide range of vapour velocities. This is in close agreement with recent rectangular channel data by *Biage /12/* but in contrast to results from circular tube tests by *Zabaras /8/*, where the Δp-increase was steeper and did not continue beyond the onset of flooding. Based on our visual observations, this difference in pressure drop characteristics is related to the fact that, in the present tests, only one of the walls is wetted by a liquid film prior to flooding, in contrast to circular tube experiments. Therefore, once disturbed flow conditions have occured near the lower channel end, a redistribution of the falling liquid film over other channel walls occurs and gradually continues over a range of vapour velocities, up to values beyond the onset of flooding. Since these competing processes of liquid redistribution and carry-over may depend on the liquid injection rate, the measured pressure drop curves are partly dependent on this rate (see figure 4). Moreover, the Δp-curves during flooding show a slight trend to higher values for the measurement position closer to the liquid feed as well as for the lower total liquid injection rates.

In contrast to the mentioned effects on the pressure gradient, the flooding curve itself is clearly independent of the liquid injection rate (see figure 3). The reason is that relatively small changes of parameters determining the pressure drop, such as the wetted circumference or the core liquid fraction, do only weakly affect the overall momentum balance solution, which is supposed to control the steady-state flooding process. This point is not outlined in detail in this paper.

4.3 Liquid Fraction

Figure 5 shows an example of a typical raw optical probe signal. The high voltage signal level signifies the presence of vapour at the probe tip, whereas the low voltage peaks indicate the passage of droplets. For each given flow operating point and probe position, the signal was recorded during a total period Δt_{tot}=18.2 s. The applied method to evaluate the wetting period Δt_i of each individual droplet and thus the local time-averaged liquid fraction is illustrated in figure 5 and based on the following concept. Once the output signal starts to decrease below the "vapour level", the considered droplet is already present at the probe tip. On the other hand, the data point, where the signal again starts to rise versus the "vapour level", is definitely the last one that may be counted as "wet", in view of possible adhesion effects between the droplet and the tip.

Figure 6 shows some liquid fraction results for various radial positions between the channel centerline and the wall, where the liquid film is supplied. The presented data refer to the lower probe position shown in figure 2. For the lateral probe positions Y=0, 5 and 7 mm, the error band with respect to these data is of the order of ±15%, due to the restricted practically feasible data recording period causing a non-ideal statistical averaging of the signal. For probe positions closer to the wall, the uncertainty range is larger, as the liquid (droplets or film) velocities are drastically decreasing. Adhesion effects between the droplets and the probe tip may cause additional errors. These are probably small because of the small probe tip, but they cannot definitely be quantified at present, since no accurate reference measurement techniques seem to be available in the considered range of very high void fractions (*Hewitt, /13/*). The specified uncertainties with respect to the presented data may thus be considered acceptable.

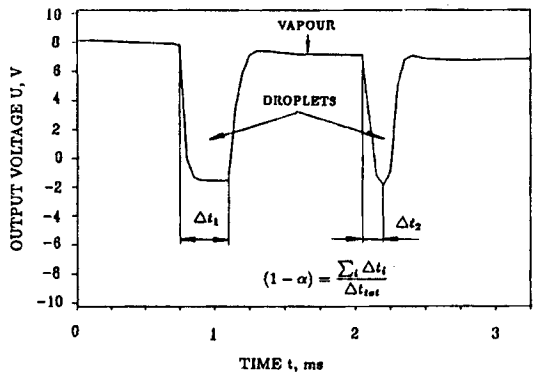

Fig.5 Typical Raw Optical Probe Signal (p=0.67 MPa, j_V=1,4 m/s, centerline position)

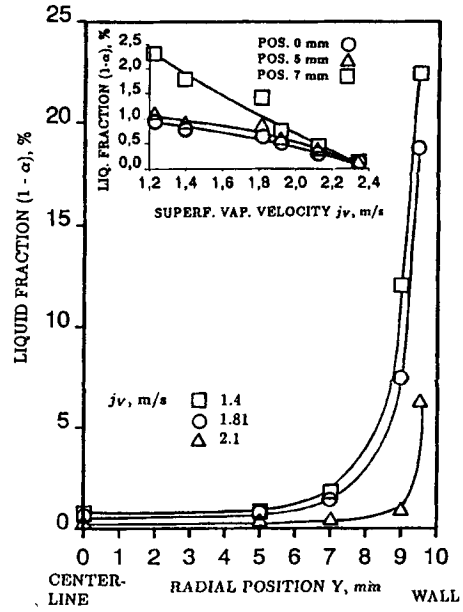

Fig.6 Liquid Fraction during Flooding (p=0.67 MPa, j_L^{IN}=0.017 m/s, upper liquid injection)

The local liquid fraction distributions shown in figure 6 clearly indicate an annular-type flow pattern, with a flat profile and very low liquid fraction values over most of the channel width. At each considered position, the liquid fraction is decreasing with increasing vapour velocity. This is in agreement with the decreasing interfacial wave amplitude found by *Zabaras /8/* and *Emmerechts and Giot /14/* from local instantaneous film thickness measurements. The evaluation of droplet sizes or velocities from optical probe data is delicate, as only wetting periods are measured and no strong correlation between droplet size and velocity seems to exist(*Azzopardi et al. /15/, Lopes /16/*). However, a conservative estimation of maximum droplet sizes is possible by calculating the product of the maximum wetting period within a signal sequence and the local gas velocity, which is the maximum possible droplet velocity. For p=0.67 MPa and the positions Y=0 mm and Y=5 mm (see figure 6), this estimation yields a maximum droplet diameter of the order of 3.5 mm.

The presented liquid fraction data are thus contradictory to the concept that steady-state single channel flooding is governed by a chaotic flow pattern with liquid bridges across the channel, as it was postulated in a number of analytical studies (*Shearer and Davidson /17/, Cetinbudaklar and Jameson /18/, Popov and Rohatgi /19/*).

5. ANALYTICAL MODEL

5.1 Formulation of the Model

Based on the above experimental evidence indicating annular flow as the pertinent flow pattern during steady-state flooding, a mechanistic core/film flow model was developed to calculate flooding. The model was formulated for circular tubes and is based on the axial momentum balance equations for a liquid wall film and a gas or va-

pour core. In calculations for non-circular channel geometries, the hydraulic diameter substitution was used. The liquid film curvature as well as radial pressure gradients and any axial gradients were neglected. A mean film thickness δ and a mean axial velocity u_G were assigned to the liquid film and to the gas within the core, respectively. The interfacial momentum exchange including all possible contributions was modeled by an empirical friction factor defined by $f_i = \tau_i/(\rho_G u_G^2/2)$. A velocity profile was taken into account within the liquid film, in order to avoid the use of purely empirical wall friction factor correlations.

Provided the core liquid fraction is known, the steady -state vertical momentum balance equations for the core and the film yield, after some manipulation, a relation of the form

$$j_L = f(j_G, \delta) \tag{1}$$

From a liquid film stability analysis, we obtain

$$(\partial\tau_i/\partial\delta)\,|_{j_L=const} = (\partial\tau_i/\partial\delta)_{j_G=const} \tag{2}$$

as a limiting condition for the existence of countercurrent flow. Since eq.(2) may be alternatively written in the form $f(j_L, j_G, \delta)=0$, the flooding curve $j_L=f(j_G)$ is determined by combining eqs.(1) and (2). The stability criterion according to eq.(2) was originally developed by *Barnea and Taitel /20/* and is equivalent to the frequently applied "envelope" approach /1/.

A physically meaningful interfacial friction factor formulation is crucial to obtain consistent flooding predictions. Based on assessment calculations, the empirical correlation used in the present study reads

$$f_i = 0.079 Re_G^{-0.25}(1 + 115\delta^{*B}) \tag{3}$$

where $B=3.95/(1.8+3.0/D^*)$. δ^* and D^* are dimensionless ratios of film thickness and tube diameter, respectively, to the Laplace length $[\sigma/(\rho_L-\rho_G)g]^{1/2}$. Eq.(3) constitutes a modification of a correlation proposed by *Barathan et al. /21/*, which has been the only published interfacial friction factor correlation for countercurrent flow. For the calculation of the liquid film velocity profile, the flow was assumed to be laminar ($\tau(y) = \eta_L(\partial u/\partial y)$). In our studies, experimental pressure drop data could generally be better predicted with this concept than by assuming various degrees of turbulence. This is in agreement with experimental results by *Maron et al. /22/* suggesting that wavy film flow may be laminar even up to relatively high Reynolds numbers.

In the present calculations, the core density was taken to be equal to the gas density, thus neglecting the core liquid fraction (1-α), which is generally not a priori known. With respect to the flooding predictions, this assumption is of negligible impact, for (1-α)-values of the order of magnitude measured in this study. However, with respect to the pressure drop, the calculated values even for such low liquid fractions, need to be corrected for the hydrostatic pressure difference due to the presence of liquid in the core flow.

5.2 Results and Discussion

Figure 7 shows calculated and measured flooding curves for the present Freon 12 tests. In figure 8, similar comparisons are presented for some atmospheric pressure tests, which have been selected according to a number of comparability criteria. The basic experimental conditions of these tests are given in the figure. In view of the various considered channel sizes and fluid properties, such as phase density ratio, surface tension and liquid viscosity, the overall prediction of the considered experimental flooding curves by the present theory is satisfactory and, moreover, significantly better than by alternatively applying the purely empirical *Wallis* and *Kutateladze* correlations .

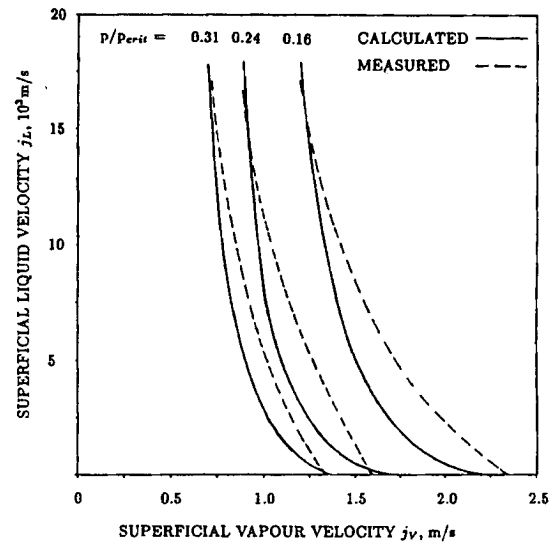

Fig.7 Comparison between Calculated and Measured Flooding Curves (Freon 12 Tests)

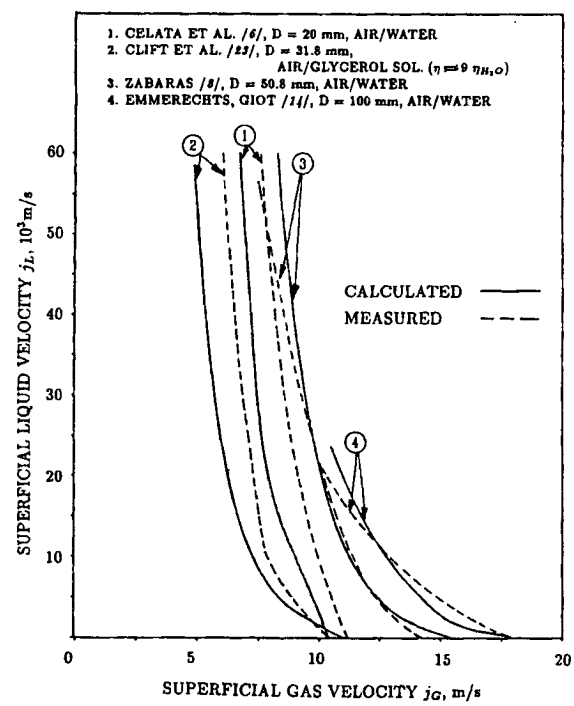

Fig.8 Comparison between Calculated and Measured Flooding Curves (Atmospheric Pressure Tests)

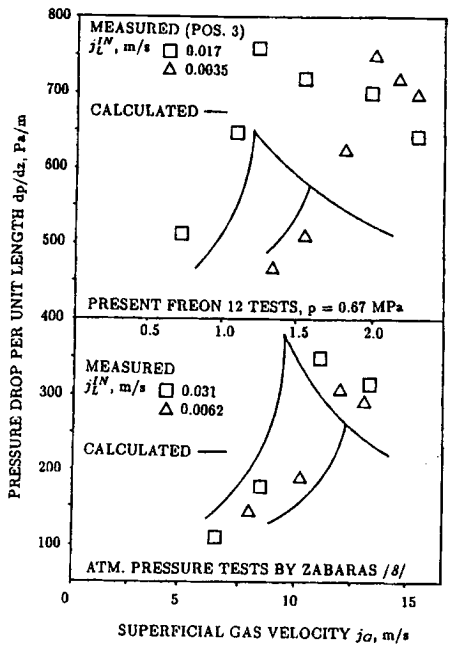

Fig.9 Comparison between Calculated and Measured Pressure Drop for High and Low Pressure Tests

Figure 9 presents pressure drop data and theoretical predictions from the above system of equations, for the present Freon 12 tests (p=0.67 MPa) and for the air/water atmospheric pressure experiments by *Zabaras /8/*. The solid lines represent the calculated Δp-curves for two different total liquid injection rates j_L^{IN}. For stable operating points prior to flooding, the two increasing branches correspond to the distinct values of j_L^{IN}, merging then into a common decreasing line for partial liquid delivery conditions. The experimental data corresponding to the same values of j_L^{IN} are shown by various symbols.

The *Zabaras* data are acceptably predicted in the calculations, whereas for the Freon test conditions the calculated Δp-values during flooding are significantly too low. This is due to the assumption of zero core liquid fraction in the calculations. For the air/water experiments by *Zabaras*, this simplification may be close to reality, since the high surface tension of water compared to Freon 12 is likely to suppress liquid entrainment, thus causing lower core liquid fraction values than in the Freon tests (*Whalley and Hewitt /24/*). For the Freon 12 test conditions, the difference between calculated and measured pressure drop during flooding (see figure 9) corresponds to an additional hydrostatic pressure difference caused by a core liquid fraction of the order of 1.5 %, which is in acceptable agreement with the liquid fraction data shown in figure 6. It is to be noted here that the average core liquid fraction cannot be accurately determined from measured local profiles like those shown in figure 6, due to the inability to evaluate the position of the core/film interface from optical probe data.

In view of the complexity of the considered flow phenomena the overall agreement between measured and theoretically predicted pressure gradient characteristics is reasonable, thus supporting the validity of the present analytical flooding model.

ACKNOWLEDGEMENT

The authors gratefully acknowledge the financial support provided by the Bundesminister für Forschung und Technologie (BMFT).

REFERENCES

/1/ Bankoff, S.G., & Lee, S.C. 1983, A Critical Review of the Flooding Literature, NUREG Rept. CR-3060.
/2/ Tien, C.L., & Liu, C.P. 1979, Survey on Vertical Two-Phase Countercurrent Flooding, EPRI Rept. NP 984.
/3/ Wallis, G.B. 1969, One-Dimensional Two-Phase Flow, pp. 336-345, McGraw-Hill, New York.
/4/ Pushkina, O.L., & Sorokin, Y.L. 1969, Breakdown of Liquid Film Motion in Vertical Tubes, Heat Transfer - Soviet Research, vol. 1, pp. 56-64.
/5/ Kröning, H. 1984, Untersuchungen von Gas/Flüssigkeits- Gegenströmung in vertikalen Kanälen, Dissertation, Universität Hannover.
/6/ Celata, G.P., Cumo, M., Farello, G.E., & Setaro, T. 1988, The Influence of Flow Obstructions on Flooding Phenomenon in Vertical Channels, ENEA Rept. RT/TERM/88/3.
/7/ Zabaras, G.J., & Dukler, A.E. 1988, Countercurrent Gas- Liquid Annular Flow Including the Flooding State, AICHE Journal 34, pp.389-396.
/8/ Zabaras, G.J. 1985, Studies of Vertical Annular Gas-Liquid Flows, Ph. D. thesis, University of Houston, Texas.
/9/ Hewitt, G.F., Lacey, P.M.C., & Nicholls, B. 1965, Transitions in Film Flow in a Vertical Tube, UKAEA Rept. AERE-R 4614.
/10/ McQuillan, K.W., Whalley, P.B., & Hewitt, G.F. 1985, Flooding in Vertical Two-Phase Flow, Int. Journal of Multiphase Flow, vol. 11, pp. 741-760.
/11/ Suzuki, S., & Ueda, T. 1977, Behaviour of Liquid Films and Flooding in Countercurrent Two-Phase Flow, Part 1: Flow in Circular Tubes, Int. Journal of Multiphase Flow, vol. 3, pp. 517-532.
/12/ Biage, M. 1989, Structure de la Surface Libre d'un Film Liquide Ruisselant sur une Plaque Plane Verticale et Soumis a un Contrecourant de Gas; Transistion vers l'Ecoulement Cocourant Ascendant, Thèse de Doctorat, Institut National Polytechnique de Grenoble, France.
/13/ Hewitt, G.F. 1982, Measurement of Void Fraction, in Handbook of Multiphase Systems, ed. Gad Hetsroni, pp. 10-21 – 10-33, McGraw Hill/Hemisphere, New York.
/14/ Emmerechts, D., & Giot, M. 1988, Film Structure and Pressure Gradient in Air/Water Countercurrent Flows, European Two-Phase Flow Group Meeting, Brussels, Paper E4.
/15/ Assopardi, B.J., Teixeira, J.C.F., & Jepson, D.M. 1989, Drop Sizes and Velocities in Vertical Annular Two-Phase Flow, Proc. Int. Conf. on Mechanics of Two-Phase Flows, Taipeh/R.O.C., pp. 261-266.
/16/ Lopes, J.C.B. 1984, Droplet Sizes, Dynamics and Deposition in Vertical Annular Flow, Ph. D. thesis, University of Houston, Texas.
/17/ Shearer, C.J., & Davidson, J.F. 1965, The Investigation of a Standing Wave due to Gas Blowing Upwards over a Liquid Film; Its Relation to Flooding in Wetted-Wall Columns, Journ. Fluid Mech. 22, pp. 321-336.
/18/ Cetinbudaklar, A.G., & Jameson, G.J. 1969, The Mechanism of Flooding in Vertical Counter-Current Two-Phase Flow, Chem. Eng. Science 24, pp. 1669-1680.
/19/ Popov, N.K., & Rohatgi, U.S. 1986, Analysis of Counter- Current Adiabatic Flow Limitation Phenomenon in Vertical Pipes, NUREG Rept. CR-4630.
/20/ Barnea, D., & Taitel, Y. 1985, Stability of Annular Flow, Int. Comm. Heat and Mass Transfer, vol. 12, pp. 611- 621.
/21/ Barathan, D., Wallis, G.B., & Richter, H.J. 1979, Air-Water Countercurrent Flow, EPRI Rept. NP 1165.
/22/ Maron, D.M., & Brauner, N. 1987, The Role of Interfacial Mobility in Determining the Interfacial Shear Factor in Two-Phase Wavy Film Flow, Int. Comm. Heat and Mass Transfer, vol. 14, pp. 45-55.
/23/ Clift, R., Pritchard, C.L., & Nedderman, R.M. 1966, The Effect of Viscosity on the Flooding Conditions in Wetted Wall Columns, Chem. Eng. Science 21, pp. 87-95.
/24/ Whalley, P.B., & Hewitt, G.F. 1978, The Correlation of Liquid Entrainment Fraction and Entrainment Rate in Annular Two-Phase Flow, UKAEA Rept. AERE-R 9187.